Research on Moving Target Imaging Method of Ship Based on Velocity Synthetic Aperture Radar

Lin Zhang and Yicheng Jiang[*]

Abstract—Surface ship imaging technology is widely used in military and civilian applications. To resolve the problem of imaging moving target positioning blur on sea surface, this paper proposes a method for estimating the velocity of moving target using velocity synthetic aperture radar (VSAR). Firstly, the paper analyzes the imaging mechanism and constraints of VSAR method and establishes an imaging model based on phased array radar for surface ships. Then, the rate-frequency estimation method of the multi-antenna image domain is used to correct the azimuth offset, and the image moisture algorithm is used to estimate Doppler frequency modulation. Therefore, the adaptive focusing of the target image is completed. Finally, this method is used to simulate and calculate the surface motion ship to realize continuous dynamic imaging of the moving ship. Compared with the traditional single-channel SAR radar and track-interfering radar (ATI) algorithm, the rate-frequency estimation algorithm solves the shortcomings of the azimuth positioning accuracy and improves the positioning performance of the moving target ship under large-area sea conditions.

1. INTRODUCTION

Imaging of marine ships is of great significance to the surveillance and security defense of marine water bodies. In particular, a rapid and fine imaging of ships moving in the sea plays an increasingly important role in military defense and civilian applications. To date, imaging of surface ships is widely achieved by the synthetic aperture radar (SAR) method. Tang et al. proposed a time-frequency analysis imaging method based on a combination of short-time Fourier transform(STFT) and complex dual apodization(CDA) to obtain images of surface ships [1]. Renga and Moccia used a Doppler centroid algorithm to achieve focusing on moving ships [2], and Ouchi and Hwang adopted a multilook cross correlation-constant false alarm rate (MLCC-CFAR) algorithm to separate ship targets from the sea [3]. Because of various constantly changing dynamic surface waves, including surges and wind waves on the surface of the sea, the image domain is distorted. Therefore, traditional imaging methods are prone to inaccurate positioning when being used to perform rapid and accurate imaging of moving ships on a wide sea area. To solve the inaccurate positioning problem, phased-array velocity synthetic aperture radar (VSAR) is widely introduced to sea surface imaging.

The imaging principle of VSAR is that an antenna array mounted on an airplane quickly and repeatedly scans the same area during flight so as to increase the coherence time for imaging. An airborne phased-array radar generates multiple reflectivity images when flying over a target scene. VSAR uses the phase difference between individual antennas of the antenna array to estimate the velocity frequency of moving targets in multiple images of the same scene so as to reposition the azimuth and achieve focusing, so that the signal-to-noise ratio of the surface moving targets in the image domain is enhanced [4, 5]. As first proposed by Friedlander and Porat, VSAR collects multichannel echoes through an array of

antennas and performs pixel vector operations in the image domain to finally achieve the testing and positioning of moving targets [6]. Lombardini et al. introduced a parameterization method into the signal processing of multibaseline along-track interferometric SAR(ATI-SAR) in conjunction with a superresolution method to estimate backscatter echo parameters of the ocean surface and conducted the adaptive implementation of optimal processing VSAR(AIOP-VSAR) to achieve moving target detection, significantly improving target detection performance of the radar with nonuniform background [7]. The introduction of algorithms for multifrequency VSAR(MF-VSAR) [8] and nonuniform linear array SAR (NULA-SAR) [9] enables VSAR to simultaneously detect and locate fast- and slow-moving targets. In view of the advanced potential of phased-array VSAR for sea surface imaging, the Naval Research Laboratory of the United States of America(NRL) has also confirmed that an X-band airborne 32-channel VSAR system can be applied to the accurate imaging of moving ships in the ocean; an actual measurement was conducted at an estuary in North Carolina on the Atlantic coast of the United States of America, and a phased-array VSAR system onboard the Saab 340 aircraft achieved imaging of a variety of moving reflectors (including ships, shoal waves, and currents) on the sea surface [10, 11].

To date, VSAR research has mainly focused on the accurate estimation of Doppler parameters of moving targets. By using an array of multiple antennas, VSAR generates multiple complex images, which contain the same static scene with moving targets and have the same magnitude. However, the images have different phases, which contain velocity information of the azimuth strip (i.e., velocity information along the direction of the radar line of sight). The VSAR method extracts velocity information from the phases and performs a discrete Fourier transform (DFT) operation on the corresponding pixels in the moving target region of each SAR image to form multiple SAR images representing different velocities. To address the problem of insufficient estimation accuracy of radial velocity, this study establishes an imaging model based on phased-array radar for surface ships. This model employs a velocity frequency estimation method of image stack domain and an image entropy algorithm to correct the azimuth shift and achieve adaptive focusing, thereby overcoming the inaccuracy problem of azimuth positioning and improving the positioning performance of the radar system for moving target ships on a large sea area.

2. VSAR IMAGING MODEL OF MOVING TARGETS

The VSAR model is shown in Fig. 1, where m antennas are placed at equal intervals d along the azimuth direction, and each antenna independently receives backscattered echoes, thereby forming a phased-array multichannel radar system. Va is along-track velocity of the point target P, and Vr is its radial velocity and defined to be positive when the target is receding from the radar along line. In the radar system, only antenna 0 transmits linear frequency-modulated signals, while all other antennas receive the echo signals of the target. On the assumption that all the received echo signals come from the same area, the collected data of the m antennas will form a stack of M SAR images, with the interval between adjacent images being $\Delta t = d/2V$, where V is the aircraft flight velocity.

The instantaneous slant range between the target P and transmitter antenna 0 is:

$$R_0\left(t_m\right) = \sqrt{\left(Vt_m - v_a t_m - X_0\right)^2 + \left(v_r t_m + Y_0\right)^2 + R_0^2} \tag{1}$$

Here, (X_0, Y_0) is the initial coordinates of the target ship at the sea surface, and R_0 is the vertical distance from the aircraft to the target.

The instantaneous slant range between the target P and receiver antenna m is:

$$R_m\left(t_m\right) = \sqrt{\left(Vt_m - v_a t_m + md - X_0\right)^2 + \left(v_r t_m + Y_0\right)^2 + R_0^2} \quad m = 0, 1, \ldots M - 1 \tag{2}$$

It is assumed that the radar system transmits linear frequency-modulated signals, the antenna m receives an echo signal of the target P and demodulates it to the baseband as expressed by Equation (3):

$$s\left(t, t_m, m\right) = A_m a_r\left(t\right) \exp\left\{j\pi\gamma\left(t - \frac{R_0\left(t_m\right) + R_m\left(t_m\right)}{c}\right)^2\right\} \cdot \exp\left(-j2\pi\frac{R_0\left(t_m\right) + R_m\left(t_m\right)}{\lambda}\right) \tag{3}$$

Here, A_m presents the reflection coefficient of the point target, and $a_r\left(t\right)$ is the antenna pattern gain.
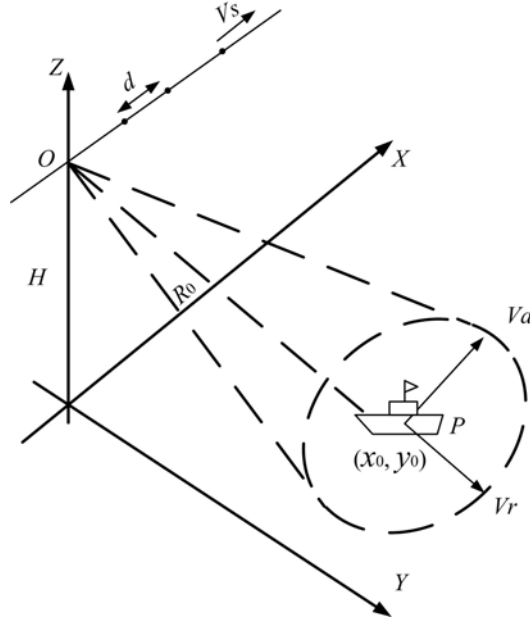
Figure 1. Schematic diagram of the VSAR model.

Accordingly, the echo signal received by antenna m from the target P can be expressed as Equation (4) after distance compression:

$$s_r(t, t_m, m) = A_m \cdot \mathrm{sin}\, c\left[B\left(t - \frac{R_0(t_m) + R_m(t_m)}{c}\right)\right] \cdot \exp\left(-j2\pi\frac{R_0(t_m) + R_m(t_m)}{\lambda}\right) \quad (4)$$

$$R_0(t_m) + R_m(t_m) = 2R_0 + 2v_r t_m + \frac{(Vt_m - v_a t_m - X_0)^2 + (Vt_m - v_a t_m + md - X_0)^2}{2R_0}$$

$$\approx 2R_0 + \frac{m^2 d^2 - 2X_0 md + 2X_0^2}{2R_0} + f_{dc}t_m + f_r t_m^2 \quad (5)$$

The Doppler centroid frequency is

$$f_{dc} = -\frac{2}{\lambda} \cdot \frac{(md - X_0)(V - v_a) + Y_0 v_r}{R_0} \quad (6)$$

Here, $f_d = -\frac{2v_r Y_0}{\lambda R_0}$ is the Doppler shift caused by the target radial velocity, while $f_0 = -\frac{(md-X_0)}{\lambda R_0}(V - v_a)$ is the Doppler shift caused by the antenna element spacing in the radar array and is usually small.

The Doppler frequency modulation is:

$$f_r = -\frac{2(V - v_a)^2 + v_r^2}{\lambda R_0} \quad (7)$$

The images obtained by VSAR are from the same scene, and therefore these images are coherent. However, the relative positions of the channels along the azimuth direction are different from one another, which causes azimuth shift between coherent images. In addition, because of jitter in the aircraft during flight, it is necessary to conduct the registration process of each image of the image stack prior to velocity estimation [12]. Only when the corresponding pixel vectors of all images originate from the same resolution cell can the images be accurately registered and the subsequent velocities of the moving target be effectively estimated. However, as a result of instantaneous surges on the sea surface, it is difficult to achieve accurate registration; therefore, the cell-averaging CFAR (CA-CFAR) detection method is employed by this study for sector imaging [13] followed by image calibration and recognition, thereby overcoming the difficulty of moving target recognition on the sea surface.

3. VSAR IMAGING ALGORITHM FOR MOVING TARGETS IN A LOCALIZED AREA

Sea surface imaging is subject to a variety of interference factors: On the one hand, when the velocity of the surface ship target is slow, the Doppler frequency of the target in the echo frequency domain is similar to that of sea clutter. Therefore, it is difficult to identify the target ship from the sea clutter spectrum by using a narrow range of Doppler frequency (typically in the range of $\pm 1.5\,\text{Hz}$). On the other hand, because of the existence of surges on the sea surface, even fast-moving ships are subject to six-dimensional micromotions of roll, pitch, and yaw, so that it is very difficult to estimate Doppler parameters of moving ships on the sea surface accurately. In addition, high-frequency radar electromagnetic waves transmitting through the unstable ionosphere are subject to multipath propagation and undergo nonlinear changes in the phase path, which generates Doppler spectrum broadening of sea clutter to further mask echo signals of slow-moving targets nearby, which in turn leads to a narrower frequency band in the frequency domain for effective target detection, causing great difficulty in the successful identification of slow-moving targets, such as ships. In short, the above-mentioned interaction between sea surface waves and ships has an adverse impact on the Doppler analysis and accurate imaging of moving targets on the sea surface.

Given that a ship moves across multiple azimuth resolution cells during the synthetic aperture period, the Doppler course of the ship is dispersed in a small local area. Therefore, the CA-CFAR detection method is used to retrieve the ship echoes on the sea surface [13]. The effect of ocean surges on the instantaneous Doppler parameters of the target is eliminated to achieve the phase compensation caused by the spacing of antennas. Next, position correlation is performed on major scattering points of each ship so that the unified attitude of the ships in the image stack during the synthetic aperture period is obtained. Based on the received signals at multiple receiver antennas, Doppler phase accumulation is estimated, which allows the radial velocity to be estimated and the moving targets to be repositioned. Finally, the Doppler frequency modulation of the target in focus is obtained by using the image entropy method [14] so that refocusing of the moving target is achieved. Superposition of the moving target in the image stack reconstructs the motion trajectory of the ship during the synthetic aperture period. The algorithm flowchart is shown in Fig. 2.
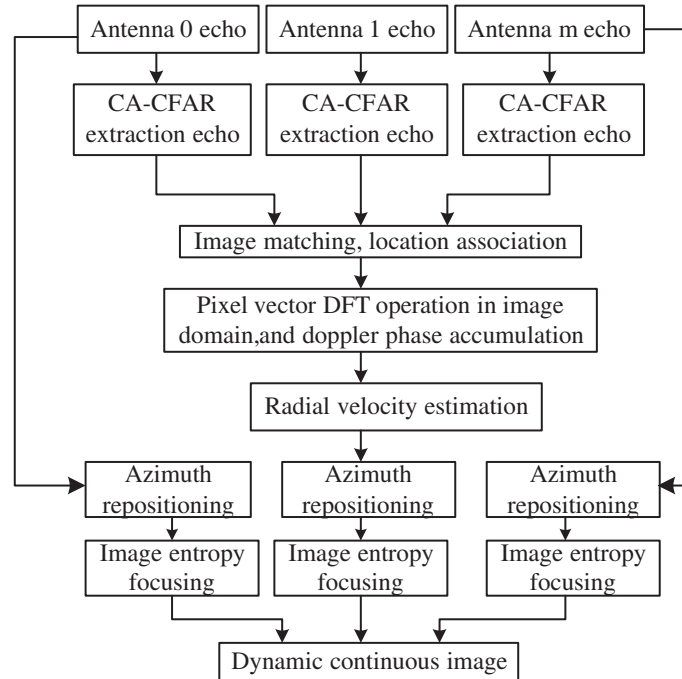

Figure 2. Flowchart of the VSAR algorithm.

3.1. CA-CFAR Detection Method

CFAR detection is suitable for detecting targets in a cluttered background. In the 1960s, Finn and Johnson were the first to propose the CA-CFAR detection method [15], and this method makes good detection performance possible in a uniform cluttered background. However, for the imaging of surface ships, the space occupied by ships in a wide sea area is relatively small, and thus, it is unrealistic to analyze globally the moving parameters of moving targets. Therefore, when analyzing the echo data in the background window, the sea surface in the window is divided into several regions, and then the CA-CFAR method is used to lock the target. The overall amplitude of sea clutter is statistically analyzed in the sea area that not only is centered on a particular detection cell, but also includes the surrounding cells, and the detection threshold is constantly updated according to the estimated variance of the noise. If there is a target ship in addition to sea waves on the sea surface, the amplitude of echoes will become larger. If a detected signal is greater than or equal to the threshold, it indicates that the moving target is detected, and in such a case, the echo of the target is retrieved — out of the echoes of the wide sea area according to the target imaging position — to use as the input data for VSAR imaging.

3.2. Radial Velocity Estimation and Moving Target Repositioning

After obtaining the echo of the target ship based on the CA-CFAR method, the image stack is registered so that the image pixels obtained by each antenna are uniformly aligned. The moving target model of each image domain of VSAR is:

$$S(m) = \sigma \exp\left[-j\frac{2\pi}{\lambda}\left(2R_0 + \frac{m^2d^2 + 2X_0^2}{2R_0}\right)\right] \cdot \exp\left(j\frac{2\pi m dX_0}{\lambda R_0}\right) \quad m = 0, 1 \ldots M - 1 \qquad (8)$$

The azimuth interval between the antennas inevitably leads to phase error between the images, and therefore, the error has to be compensated according to the following compensation model:

$$S_1(m) = S(m) \cdot \exp\left(j\frac{2\pi}{\lambda} \cdot \frac{m^2d^2}{2R_0}\right) = \sigma \cdot \exp\left(-j\frac{4\pi}{\lambda}R_0 - j\frac{2\pi X_0^2}{\lambda R_0}\right) \cdot \exp\left(j\frac{2\pi m dX_0}{\lambda R_0}\right) \qquad (9)$$

Because $X_0 \ll R_0$, the phase term $\left(-j\frac{2\pi X_0^2}{\lambda R_0}\right)$ due to the target azimuth position is negligible, and, accordingly, the above formula can be reduced to:

$$S_2(m) = \sigma\left(-j\frac{4\pi}{\lambda}R_0\right) \cdot \exp\left(j\frac{2\pi m dX_0}{\lambda R_0}\right) \qquad (10)$$

X_0 in the above formula contains the azimuth shift Δ_{shift} due to the moving target, with $X_0 = X'_0 + \Delta_{shift}$, where X'_0 is the abscissa position after the target moves. Therefore, the expression of the azimuth shift of the moving target is:

$$S_3(m) = \sigma\left(-j\frac{4\pi}{\lambda}R_0\right) \cdot \exp\left(-j\frac{2\pi m d\Delta_{shift}}{\lambda R_0}\right) = \sigma\left(-j\frac{4\pi}{\lambda}R_0\right) \cdot \exp\left(j2\pi m f_v\right) \qquad (11)$$

As shown by $f_v = -\frac{d\Delta_{shift}}{\lambda R_0}$, there is a relationship between the velocity frequency and the azimuth shift:

$$\Delta_{shift} = -\frac{\lambda R_0}{d} \cdot f_v \qquad (12)$$

In the meantime, the azimuth shift of the moving target can be expressed as:

$$\Delta_{shift} = v_s \cdot \frac{f(t_m)}{f_r} = v_s \cdot \frac{[(2X_0 + md) \cdot v_a + 2Y_0v_r]/R_0}{2v_s^2/R_0} \approx \frac{X_0v_a + Y_0v_r}{v_s} \qquad (13)$$

If the velocity frequency is precisely known, it is possible to derive the azimuth shift from the above formula so as to realize moving-target repositioning. Therefore, the spatial steering vector of the moving target in the VSAR system model is:

$$a(f_v) = [1, \exp(j2\pi f_v), \exp(j2\pi \cdot 2f_v), \ldots \exp(j2\pi(M-1)f_v)]^T \qquad (14)$$

To obtain an estimate of the moving target velocity frequency, an M-point DFT is performed on the same element of the M images along the direction of the antenna array, that is, each pixel in the predetermined image is processed laterally. Specifically, echo signals received by all the antennas in the array are combined to form a set of independent three-dimensional images $\{Y_m(x,y), m = 0, 1 \ldots M-1\}$, after which velocity processing is conducted along the antenna direction to finally generate $Z(x,y,v)$, which is an image that provides three-dimensional resolutions in azimuth/distance/velocity for the same target scene. After all the pixels are processed, the phase difference of received echo signals between multiple antennas is used to derive a smooth velocity frequency f_v, after which the azimuth shift Δ_{shift} is derived according to Equation (12) so that the target is repositioned. Given that the algorithm does not process a large sea area but only deals with small-area echo components after CFAR detection, the computation volume and time are acceptable. In VSAR processing, spectral analysis techniques are used to generate multiple images representing different velocity intervals, and each target at different velocities is allowed to fall in a different velocity interval, followed by superposing the targets within all velocity intervals to form a set of all ship targets.

3.3. Estimation of Doppler Frequency Modulation and Moving Target Refocusing Based on the Adaptive Image Entropy Method

The radial velocity of the moving target causes Doppler centroid shift, which leads to azimuth shift of the target in the SAR image. The velocity of the moving target along the azimuth direction shows a certain degree of spectral broadening in the azimuth direction after pulse compression, and the broadening causes image defocusing and image resolution degradation. Therefore, the Doppler frequency modulation is closely related to the azimuth velocity of the moving target. The dynamic ocean surface has a complex environment. First, the surface surge velocity can be as high as several meters per second, and it shows a certain degree of nonlinearity; second, wind undergoes instantaneous changes along a number of different directions, especially near the coast where the wave spectrum becomes narrower, and the wave steepness increases, and thus, it is especially difficult to achieve shoal wave imaging near the coast [16]. It is very difficult for single-channel SAR to achieve image focusing and azimuth repositioning of a moving target. In a sea scene detected by a multiantenna radar system, waves and ships are moving, and to achieve refocusing of a moving target, it is necessary to allow multiple channels to undergo adaptive self-focusing.

The image entropy method has a wide range of applications for Doppler frequency modulation estimation of targets, which can be independent of any echo data model, and does not require the existence of strong point targets. Therefore, from the complex image domain, the image entropy method is used to focus the data of each receiving antenna adaptively. The image entropy can be defined as:

$$E(I) = -\sum_{m=0}^{Na-1}\sum_{n=0}^{Nr-1} \rho(m,n) \lg \rho(m,n) \tag{15}$$

where $0 \le m \le Na-1$, m is the azimuth pulse index, Na the number of azimuth pulses, $0 \le n \le Nr-1$, n the range unit index, and Nr the number of range units.

$\rho(m,n)$ is the scattering intensity density of the image:

$$\rho(m,n) = \frac{|I(m,n)|^2}{P(I)} \tag{16}$$

where $I(m,n)$ is the image complex scattering intensity, and $P(I) = \sum_{m=0}^{Na-1}\sum_{n=0}^{Nr-1} |I(m,n)|^2$ is the total energy of a given radar image and is a constant.

In this study, the image data of each receiver antenna in the complex image domain are subject to adaptive self-focusing based on the image entropy method. First, the echo components of the target are subject to range compression, and a traversal search of Doppler frequency modulation is performed on the images that undergo range migration compensation based on the keystone transform. Next, the range of Doppler frequency modulation is determined by formula (13) to complete the rough search and imaging process. In the range of target imaging region determined in Section 3.1, the Doppler

modulation frequency is estimated, and the azimuth matching reference function is constructed to achieve fine focusing. In the process of estimation, image entropy algorithm is used to search Doppler parameters step by step, and the parameters in the most focused state of the image are obtained, so that the phase error of the azimuth direction of the echo signal is minimized. Given that sea waves are temporally correlated in the azimuth direction, it is possible to derive the azimuth velocities of a moving target through a fitting of the Doppler frequency modulation.

4. SIMULATION EXPERIMENT AND RESULT ANALYSIS

To verify the effectiveness of the VSAR algorithm, sea waveforms under different sea conditions were constructed, and the effects of surges on the imaging of a moving target on the sear surface were analyzed. A sea wave spectrum is a power density spectrum of the sea surface, which reflects how the fluctuations of sea surface height are statistically distributed in terms of wave wavelength and wave propagation direction. In this study, wind waves and surges were superimposed to construct sea surface waves, and the amplitude of the waveform was subject to fast Fourier transformation, whereby the time-dependent frequency components of the ocean waves in the spatial domain were calculated, so that the variation characteristics of the ocean waves on the spatial scale and temporal scale could be obtained.

In this paper, we adopt the wind wave spectrum model based on wavenumber domain proposed by Donelan and Pierson [17], in which the wave number and direction relative to wind direction are used as parameters, and the power spectral density function of wave height on the ocean surface caused by wind force is given. Because of inertia and gravity, the surge model, which keeps the sea surface vibrating, adopts the Gaussian [18]. The total ocean wave spectrum consists of wind wave spectrum and surge spectrum. Considering the random phenomenon of sea surface, the surface amplitude of ocean wave obeys Rayleigh distribution. The total ocean wave spectrum is transformed by fast Fourier transform, and the height spectrum of sea surface wave is obtained. The sea surface area simulated in this study was $15000\,\text{m} \times 15000\,\text{m}$ with 600×600 grid points, and the wind direction angle was set to $45°$. A three-dimensional wave surface was simulated under two different sea conditions.

By comparing the simulation results of Figure 3 and Figure 4, it is revealed that wind speed directly affects the fluctuations of wave peaks and troughs. When the wind speed is low, the sea surface fluctuations are relatively stable and not large. As the wind speed increases, the sea wave spectrum undergoes changes more frequently so that the degree of temporal correlation decreases, with the peaks and troughs instantaneously alternating. Figure 5 shows a grayscale image of the three-dimensional sea surface wave spectrum. Imaging of a moving target ship with phased-array VSAR was simulated based on the simulation parameters listed in Table 1. The simulation scene was set to have a moving ship in the sea.

Given the false alarm probability, the echo of the ship target can be extracted by CA-CFAR algorithm. The location of the target is in the center of the echo data as shown in Fig. 6. Then in
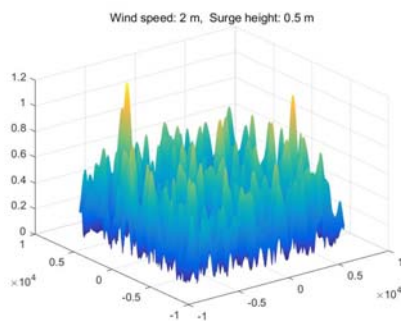

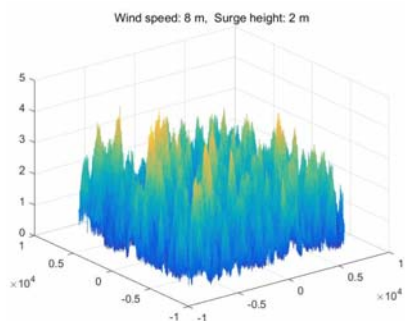**Figure 3.** Three-dimensional sea surface under low sea condition.

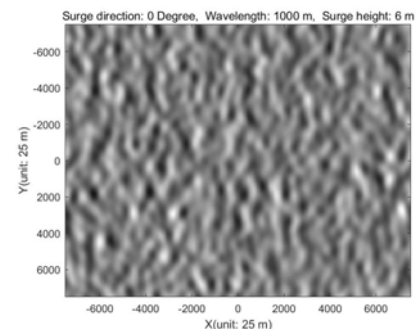**Figure 4.** Three-dimensional sea surface under high sea condition.

**Figure 5.** Simulated sea surface.

Table 1. Simulation parameters for a ship on the sea surface.

Carrier frequency (GHz)	1.5	Transmitter pulse duration (µs)	1.5
Slant range (km)	3	Transmitter pulse bandwidth (MHz)	150
Carrier velocity (m/s)	300	A/D sampling rate (MHz)	256
Number of phased-array antennas	10	Ship initial coordinates (X, Y)	(10, 50)
Antenna spacing (m)	6	Ship radial velocity (Vr) (m/s)	6
PRF (Hz)	384	Ship along velocity (Va) (m/s)	20
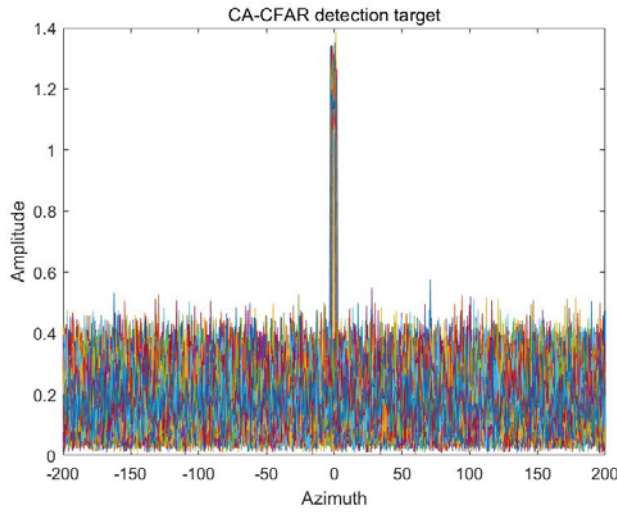
Figure 6. CA-CFAR detection of ship targets.
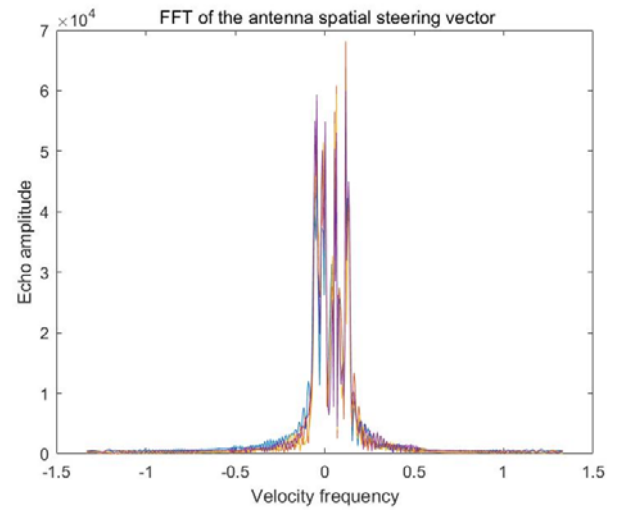
Figure 7. Velocity frequency spectrum of the spatial steering vector of antenna array.

the image domain, the velocity frequency of the elements is estimated in the spatial domain along the direction of the antenna array, and a velocity frequency spectrum is obtained as shown in Fig. 7. Here, take the equally spaced antennas 1, 4, 7, and 10 as an example. As shown in the figure, the velocity frequency with 10 antennas is $10f_v \approx 0.16\,\text{Hz}$. Given that the antennas are equally spaced, calculation based on Equation (14) gives $f_v = 0.016\,\text{Hz}$, which is then substituted in Equation (12) to derive the azimuth shift of 1.6 m. However, the theoretical azimuth shift is predicted to be 1.67 m according to Equation (13), suggesting that the accuracy of this algorithm is high enough for predicting the azimuth shift of a moving target.

Figure 8 shows that in the images generated by antennas 1, 4, 7, and 10, the ship position has been corrected so that the motion direction and trend of the ship are clearly revealed, thereby enabling the ship velocity to be perceived in a more intuitive manner. Fig. 9 presents a simulated trajectory of a moving ship on the sea surface. Through the analysis of the above two graphs, when the ship moves along the diagonal line, it can be decomposed into the superposition of the azimuth and range motion. The range motion can be determined by the VSAR method in this paper. The azimuth motion (along the flight) can correct the image defocusing by the image moisture algorithm. As shown in Figs. 8 and 9, phased-array radar is superior to single-channel radar in the imaging of moving targets — that is, the former can achieve continuous dynamic imaging of moving targets in a short synthetic aperture period without additional data so that it is beneficial for predicting the velocities, directions, and positions of target ships.
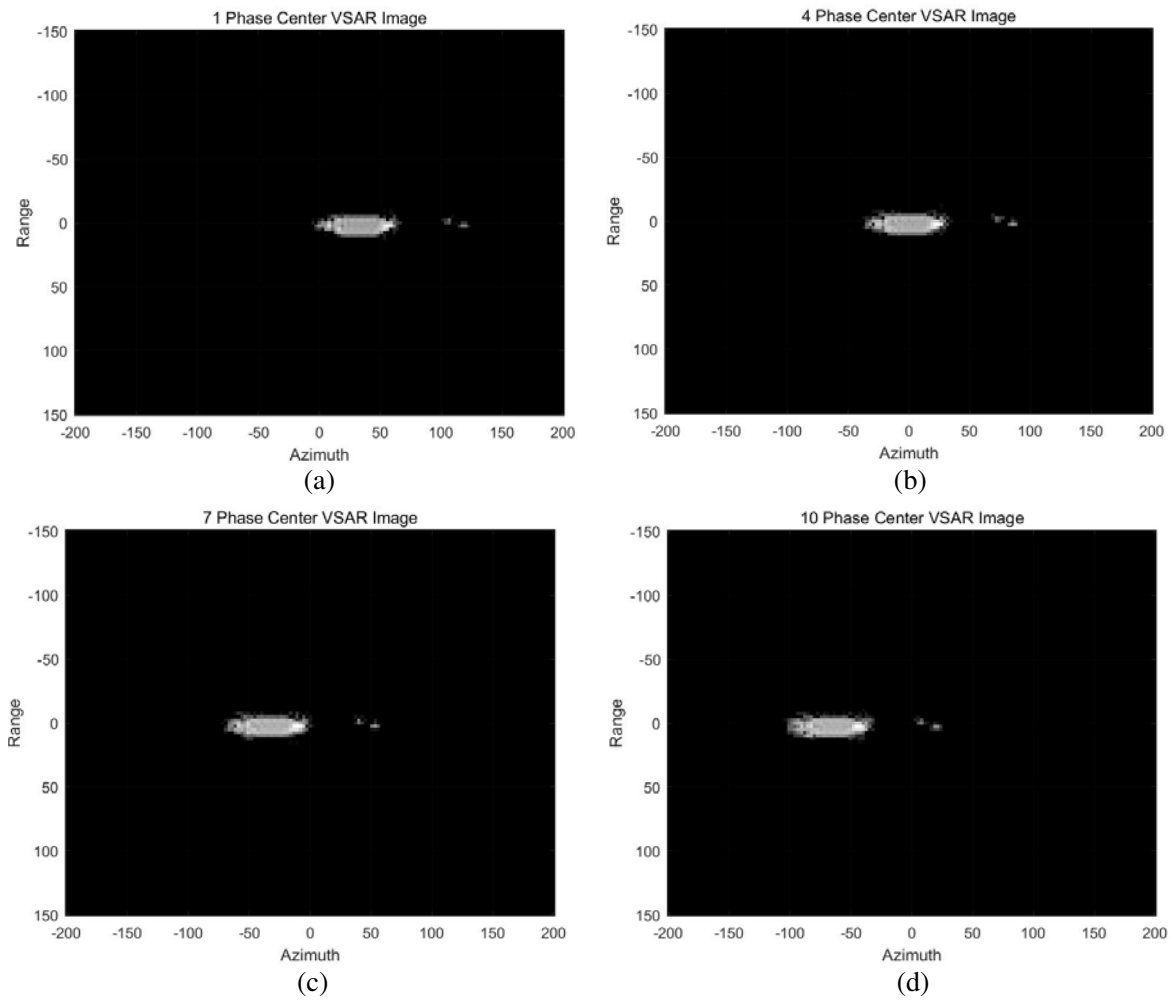
Figure 8. Imaging by equally spaced antennas of the antenna array. (a) VSAR imaging by Antenna 1. (b) VSAR imaging by Antenna 4. (c) VSAR imaging by Antenna 7. (d) VSAR imaging by Antenna 10.
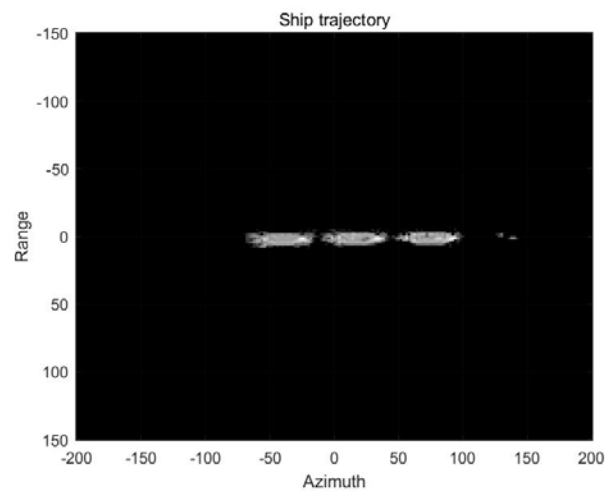

Figure 9. Ship trajectory imaging.

5. CONCLUSION

A theoretical analysis and simulation of the VSAR imaging model of moving targets were performed, and it is found that phased-array VSAR processing is a good choice for the imaging of small moving targets, such as ships in a wide sea area. The method can realize continuous dynamic imaging of moving targets in a short synthetic aperture period, which plays a pivotal role in judging ship motion trends and navigation trajectories. Incorporation of the CA-CFAR algorithm in the VSAR model can overcome the difficulty in processing a large volume of data of a wide sea area, and echo data analysis of local regions can help to mitigate the defocusing effect of sea clutter on ships, all of which provide reference value for practical applications.

ACKNOWLEDGMENT

REFERENCES

1. Tang, L.-B., D.-J. Li, Y.-R. Wu, et al., "High resolution SAR imaging of moving ship targets at sea," *Journal of Electronics & Information Technology*, Vol. 28, No. 4, 624–627, 2006.
2. Renga, A. and A. Moccia, "Use of doppler parameters for ship velocity computation in SAR images," *IEEE Transactions on Geo-Science and Remote Sensing*, Vol. 54, No. 7, 3995–4011, 2016.
3. Ouchi, K. and S.-I. Hwang, "Improvement of ship detection accuracy by SAR multi-look cross-correlation technique using adaptive CFAR," *IEEE International Geoscience & Remote Sensing Symposium, IEEE*, 3716–3719, 2010.
4. Jansen, R. W., R. G. Raj, L. Rosenberg, and M. A. Sletten, "Practical multichannel SAR imaging in the maritime environment," *IEEE Transactions on Geoscience and Remote Sensing*, Vol. 56, No. 7, 4025–4036, 2018.
5. Li, G., J. Xu, Y.-N. Peng, and X.-G. Xia, "Velocity layover solution in VSAR image," *2006 CIE International Conference on Radar*, 16–19, Shanghai, China, 2006.
6. Friedlander, B. and B. Porat, "VSAR: A high resolution radar system for detection of moving targets," *IEE Proceedings-Radar, Sonar and Navigation*, Vol. 144, No. 4, 205–218, Aug. 1997.
7. Lombardini, F., F. Bordoni, F. Gini, et al., "Multibaseline ATI-SAR for robust ocean surface velocity estimation," *IEEE Transactions on Aerospace and Electronic Systems*, Vol. 40, No. 2, 417–433, 2004.
8. Wang, G., X.-G. Xia, and V. C. Chen, "Multi-frequency VSAR imaging of moving targets," *Radar Processing, Technology and Applications IV*, 159–169, Denver, CO, United States, September 1999.
9. Gang, L., X. Jia, Y.-N. Peng, and X.-G. Xia, "Location and imaging of moving targets using nonuniform linear antenna array SAR," *IEEE Transactions on Aerospace and Electronic Systems*, Vol. 43, No. 3, 1214–1220, 2007.
10. Sletten, M., S. Menk, J. Toporkov, et al., "The NRL multi aperture SAR system," *2015 IEEE Radar Conference*, 0192–0197, Arlington, VA, USA, May 2015.
11. Sletten, M. A., L. Rosenberg, S. Menk, et al., "Maritime signature correction with the NRL multichannel SAR," *IEEE Transactions on Geoscience and Remote Sensing*, Vol. 54, No. 11, 6783–6790, 2016.
12. Li, X. and X.-G. Xia, "Location and imaging of elevated moving target using multi-frequency velocity SAR with cross-track interferometry," *IEEE Transactions on Aerospace and Electronic Systems*, Vol. 47, No. 2, 1203–1211, 2011.
13. Li, J.-J., S.-Y. Wang, and W.-L. Hu, "Adaptive cell average CFAR detection based on multi-clutter distribution model," *Journal of Air Force Radar Academy*, Vol. 19, No. 3, 4–7, 2005.

14. Xiao, J., X.-C. Hu, H. Zhang, et al., "Estimation of the doppler frequency modulation ratio based on minimum entropy criteria for highly squinted SAR," *Modern Radar*, Vol. 35, No1, 46–54, 2013.

15. Finn, H. M. and R. S. Johnson, "Adaptive detection mode with threshold control as a function of spatially sampled clutter-level estimates," *Rca Review*, Vol. 29, No. 9, 414–464, 1968.

16. Xiong, Y.-F., Z.-G. Shi, J. Guo, et al., "Sea surface modeling based on the spectrum of ocean waves modeling and the FFT," *Journal of Chongqing University of Technology (Natural Science)*, Vol. 28, No. 4, 77–82, 2014.

17. Donelan, M. A. and W. J. Pierson, "Radar scattering and equilibrium ranges in wind-generated waves with application to scatterometry," *Journal of Geophysical Research Oceans*, Vol. 92, No. C5, 4971–5029, 1987.

18. Durden, S. and J. Vesecky, "A physical radar cross-section model for a wind-driven sea with swell," *IEEE Journal of Oceanic Engineering*, Vol. 10, No. 4, 445–451, 1985.